Terahertz transmission ellipsometry of vertically aligned multi-walled carbon nanotubes

M. J. Paul,[1] N. A. Kuhta,[1] J. L. Tomaino,[1] A. D. Jameson,[1] L. P. Maizy,[1] T. Sharf,[1] N. L. Rupesinghe,[2] K. B. K. Teo,[2] S. Inampudi,[3] V. A. Podolskiy,[3] E. D. Minot,[1] and Yun-Shik Lee[1,a)]
[1]*Department of Physics, Oregon State University, Corvallis, Oregon 97331-6507, USA*
[2]*AIXTRON Ltd., Buckingway Business Park, Anderson Road, Swavesey, Cambridge CB24 4FQ, United Kingdom*
[3]*Department of Physics and Applied Physics, University of Massachusetts Lowell, Lowell, Massachusetts 01854, USA*

(Received 8 August 2012; accepted 28 August 2012; published online 12 September 2012)

We demonstrate time-resolved terahertz transmission ellipsometry of vertically aligned multi-walled carbon nanotubes. The angle-resolved transmission measurements reveal anisotropic characteristics of the terahertz electrodynamics in multi-walled carbon nanotubes. The anisotropy is, however, unexpectedly weak: the ratio of the tube-axis conductivity to the transverse conductivity, $\sigma_z/\sigma_{xy} \cong 2.3$, is nearly constant over the broad spectral range of 0.4–1.6 THz. The relatively weak anisotropy and the strong transverse electrical conduction indicate that THz fields readily induce electron transport between adjacent shells within multi-walled carbon nanotubes. [http://dx.doi.org/10.1063/1.4752158]

Carbon nanotubes (CNTs) have exceptional electrical and optical properties which have inspired unique applications in nanoscale optoelectronics.[1–3] In particular, the electrodynamics of CNTs at terahertz (THz) frequencies are of great interest not only for fundamental materials research but also for practical applications such as high-speed electronics and biomedical sensing.[4–7] A CNT can behave as a semiconductor, semi-metal, or metal depending on its structure, yet in the THz band the optical responses are dominated by metallic CNTs while those from semiconducting CNTs are negligible. THz studies of CNT thin-films have shown strong responses to broadband THz radiation demonstrating their metallic nature.[8–10] Furthermore, the one-dimensional character of single-walled CNTs (SWCNTs) leads to strongly anisotropic THz absorption in aligned SWCNT films.[11,12] Exploiting the THz anisotropy, aligned SWCNT thin-films are shown to be excellent broadband THz polarizers.[13–15]

In this letter, we present a detailed study of the anisotropic electrodynamics in multi-walled CNTs (MWCNTs), utilizing free-space THz transmission ellipsometry. The anisotropic nature of MWCNTs is shown to be markedly different from that of SWCNTs because of electron transport between neighboring shells.

We performed angle-resolved THz transmission measurements on vertically aligned MWCNTs (V-MWCNTs), simultaneously showing the THz responses along the CNT axis (*z*-axis) and the horizontal direction (*xy*-axis). A forest of vertically aligned CNTs is an ideal black material in the visible and infrared bands, absorbing light perfectly at all angles.[16,17] Our V-MWCNT samples also show near perfect blackness by visual inspection. The perfect blackness, however, disappears in the THz region because the spacing between adjacent CNTs (~100 nm) is negligible compared with the wavelength of THz radiation. The V-MWCNT film responds to the THz wave like a homogeneous medium. In fact, THz absorption in the V-MWCNTs is substantial, but not perfect. The most surprising result of our observation is that the THz response perpendicular to the CNT axis is considerably strong, indicating electron transport between neighboring shells. The average spacing between the V-MWCNT (~100 nm) is much greater than the average CNT diameter (10–20 nm), therefore, we conclude that the THz response perpendicular to the CNT axis is due to intershell transport inside isolated V-MWCNTs. Several theoretical studies calculating intershell conduction have produced a wide variety of results depending on the detailed conditions and assumptions of the models.[18–23] An indirect experimental observation implies weak intershell conductance, yet the result is inconclusive.[24] Our direct THz conductivity measurements with a non-contact THz probe clearly resolve the strong electron transport perpendicular to the CNT axis.

The V-MWCNT samples were prepared by low-pressure chemical vapor deposition (Black Magic, AIXTRON) with 2-nm Fe on 10-nm Al_2O_3 catalyst on high-resistivity Si substrate. Individual CNTs are multi-walled, semi-metallic conductors.[25] Four samples were fabricated with varying thickness: 0 μm (no CNT deposition), 21.5 μm, 62.5 μm, and 132 μm. The CNT includes 5–15 nested cylinders, and the CNT diameter is 10-20 nm. The intershell spacing should be 0.34–0.36 nm.[26] The average spacing between neighboring CNTs is ~100 nm. Figure 1(a) shows an SEM image of the 21.5-μm thick V-MWCNT film on a Si substrate. The MWCNTs of uniform height are well-aligned in the vertical direction. We measured the angle-resolved transmission of broadband THz pulses through the samples employing free-space THz time-domain spectroscopy (THz-TDS) which provides a non-destructive probe for local carrier dynamics of metallic thin films.[27,28] The THz pulses (central frequency, 1 THz; bandwidth, 1.5 THz) were generated via optical rectification in a 1-mm ZnTe crystal. Our femtosecond laser system

a)Electronic mail: leeys@physics.oregonstate.edu.

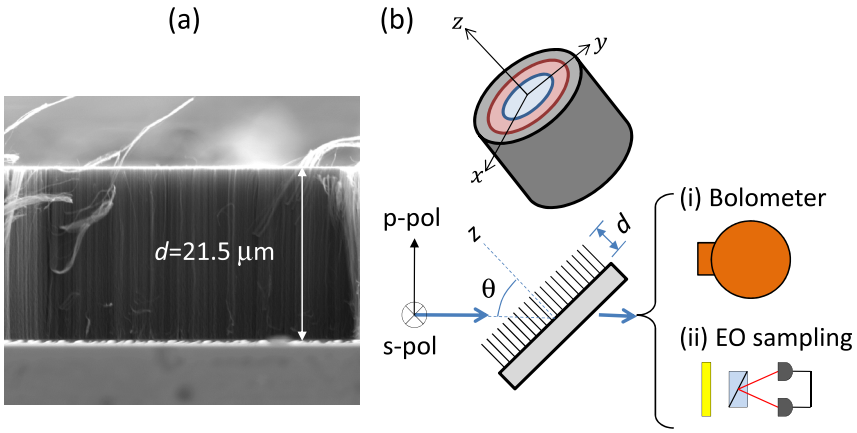

FIG. 1. (a) SEM image of the CNT-on-Si sample for the film thickness, $d = 21.5\,\mu$m. (b) Ellipsometry schematic for THz transmission measurements: linearly polarized (s-pol or p-pol), broadband pulses are incident (angle, θ) upon a V-MWCNT film on a Si substrate. THz detection schemes: (i) integrated power spectrum measured with a Si:Bolometer and (ii) THz-TDS measured with EO sampling.

is a 1-kHz Ti:sapphire amplifier (Legend, Coherent, Inc; wavelength, 800 nm; pulse energy, 1 mJ; pulse duration, 90 fs). The THz pulses were spatially focused onto the CNT-on-Si samples with parabolic mirrors (beam size, 0.5 mm). Figure 1(b) illustrates a transmission ellipsometry schematic where the THz field is oriented parallel (perpendicular) to the plane of incidence for p-polarization (s-polarization). We measured (1) spectrally integrated THz transmittance with a L-He cooled Si:Bolometer and (2) time-resolved electric-field waveforms using THz-TDS under N_2 purge with the electro-optic (EO) sampling of a 150-μm ZnTe crystal.

Figure 2 shows the spectrally integrated THz transmission through the four samples with varying CNT length for s- and p-polarization as a function of incident angle (θ). Transmission through the Si substrate with a catalyst layer ($d = 0\ \mu$m, red dots) is consistent with the calculation for a bare Si substrate ($n_{Si} = 3.42$, black solid lines), indicating the THz response to the catalyst layer is negligible. The s-pol transmission, depending only on the xy-conductivity, diminishes with increased thickness (skin depth $\sim 100\,\mu$m) and follows the typical trend of monotonic decrease with θ. The most notable feature in Fig. 2 is that the p-pol transmission undergoes pronounced changes in curvature, depending on the film thickness. It is nearly flat, yet s-shaped for $d = 62.5\ \mu$m, and monotonically decreasing for $d = 132\ \mu$m as θ increases. This peculiar angle dependence of the p-pol transmission implies that the V-MWCNTs anisotropically respond to the THz radiation, because p-pol transmission of multi-layer structures consisting of isotropic dielectric media monotonically increases until a large angle (typically $>70^\circ \sim$ Brewster angle). A detailed spectral analysis utilizing THz transmission ellipsometry will confirm that the angle-dependent trends are caused by anisotropy.

To gain more insight into the vertical and horizontal carrier dynamics of the V-MWCNT films, we performed time-resolved THz ellipsometry to obtain a time-dependent transmission function for both s- and p-polarization, $t_{s,p}(t, \theta)$. Figures 3(a)–3(d) show the directly transmitted waveforms with p-polarization through each CNT sample at $\theta = 0^\circ$, $10^\circ, 20^\circ, 30^\circ, 40^\circ, 50^\circ$, and 60°, measured by THz-TDS. The incident-angle dependence of each transmitted waveform has been normalized to the relative power transmission to remain consistent with the power transmission measurements shown in Fig. 2. A Fourier transform of the THz-TDS data

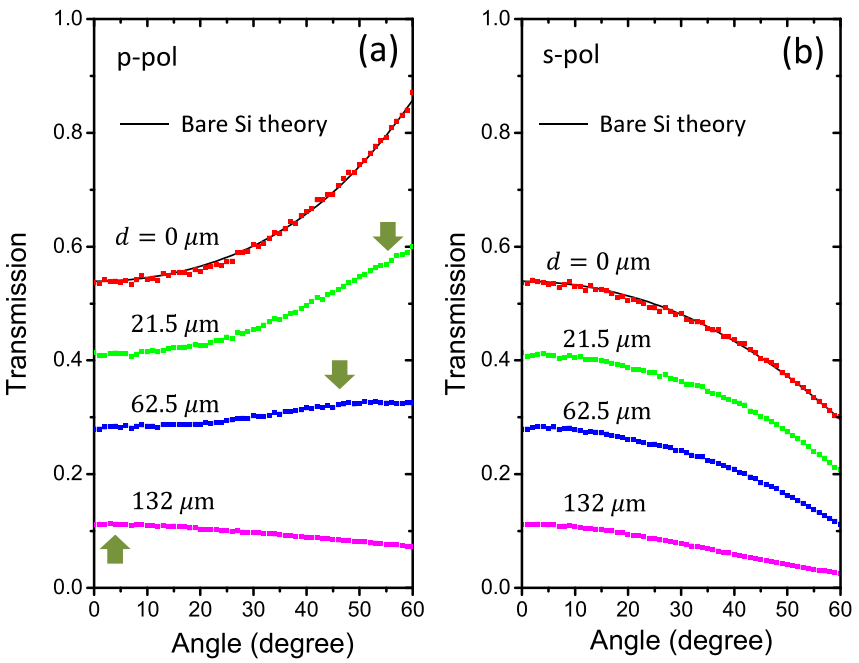

FIG. 2. Spectrally integrated THz power transmitted through the CNT samples vs. incident angle θ for (a) p- and (b) s-polarizations. The solid black lines represent the theoretical transmission for a bare-Si substrate.

yields the transmission spectrum, $t_{s,p}(\nu,\theta)$, which is compared to a uniaxial Drude-Lorentz model.

To model the polarization dependent transmission through uniaxial anisotropic layers, we use Maxwell's equations along with the continuity of electric and magnetic fields parallel to interface boundaries to obtain a transfer matrix for the amplitude coefficients $a_j^{(\pm)}$ representing the total electric-field amplitudes for forward $(+)$ and backward $(-)$ moving monochromatic waves in the j-th material region:[29]

$$\begin{pmatrix} a_{j+1}^{(-)} \\ a_{j+1}^{(+)} \end{pmatrix} = \beta \begin{pmatrix} (1+\kappa_j)\phi_j^- & (1-\kappa_j)\phi_j^+ \\ (1-\kappa_j)/\phi_j^+ & (1+\kappa_j)/\phi_j^- \end{pmatrix} \begin{pmatrix} a_j^{(-)} \\ a_j^{(+)} \end{pmatrix}, \quad (1)$$

where the polarization dependent parameters are

$$\begin{aligned} \beta_s &= \frac{1}{2}, \quad \beta_p = \frac{1}{2}\sec\theta_{j+1}\cos\theta_j, \\ \kappa_j^s &= \frac{k_z^{(j)}}{k_z^{(j+1)}}, \quad \kappa_j^p = \frac{\epsilon_{xy}^{(j)} k_z^{(j+1)}}{\epsilon_{xy}^{(j+1)} k_z^{(j)}}, \\ \phi_{j,s}^{\pm} &= \exp\left\{ i\frac{\omega}{c}\left(k_{z,s}^{(j+1)} \pm k_{z,s}^{(j)}\right) z_j \right\}, \\ \phi_{j,p}^{\pm} &= \exp\left\{ i\frac{\omega}{c}\left(k_{z,p}^{(j+1)} \pm k_{z,p}^{(j)}\right) z_j \right\}, \end{aligned} \quad (2)$$

with the dispersion relations

$$\begin{aligned} &\text{(p-pol)}\ \frac{k_x^2}{\varepsilon_z} + \frac{k_z^2}{\varepsilon_{xy}} = \frac{\omega^2}{c^2}, \\ &\text{(s-pol)}\ k_x^2 + k_z^2 = \varepsilon_{xy}\frac{\omega^2}{c^2}. \end{aligned} \quad (3)$$

The transfer matrix describes the coupling between fields in the j and $j+1$ material regions, which meet at interface position z_j. Although there are multiple transmitted exit pulses due to the internal reflections within the Si substrates, they are temporally separated and do not interfere. Only the Fourier spectrum of the first transmitted pulse is used to model numerically the THz response, measured in experiments.

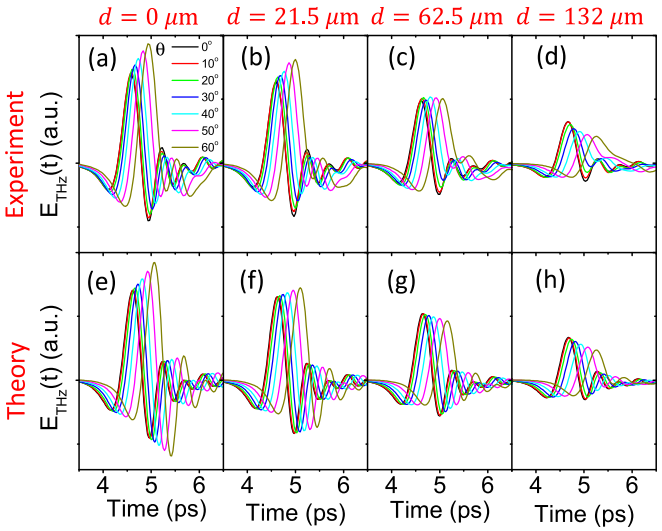

FIG. 3. P-polarization THz waveforms transmitted through the CNT samples for incident angles between 0° and 60° (a)–(d) experiment and (e)-(h) theory.

Using Eq. (1) above, the transmission coefficient for the first exit pulse is $t = t_{Air-CNT-Si} \cdot t_{Si-Air}$.

The vertical CNT film is modeled as a planar uniaxial dielectric material with polarization that is governed by independent damped-driven oscillator dynamics,

$$\epsilon_\alpha = \epsilon_\alpha^\infty - \frac{b_\alpha^2}{\omega^2 + i\omega\Gamma_\alpha - \omega_\alpha^2}, \quad \alpha = xy, z \quad (4)$$

where ϵ_α^∞ is the high frequency permittivity limit, b_α is proportional to the oscillator strength (or plasma frequency for metals), $\omega = 2\pi\nu$ is the applied angular frequency, $\omega_\alpha = 2\pi\nu_\alpha$ is the resonant angular frequency, and damping parameter Γ_α dictates the electron scattering rate. We note that the Lorentz-type dispersion model is sufficient to describe the optical properties of the CNT/air composite system. We did not employ effective medium theory because a CNT is only a few atomic layers thick and therefore an effective permittivity of a single CNT cannot be naturally introduced.

The oscillator parameters were extracted by minimizing the difference between the measured and modeled blank-normalized transmitted intensity spectrum using a Nelder-Mead nonlinear least squares algorithm.[30,31] All CNT lengths were fit simultaneously. First, s-polarized data were used to extract ϵ_{xy} parameters, then ϵ_z parameters were extracted using both p-polarized experimental data and the ϵ_{xy} result. This process was performed over the FWHM of the incident electric-field spectrum (0.4-1.6 THz). The results for the oscillator parameters are listed in Table I. The z-axis parameter $\nu_z = 0$ indicates that CNT-axis conduction is purely due to free charge carriers, while the nonvanishing xy-axis resonant frequency ($\nu_{xy} = 2.2$ THz) implies that intershell conduction is not Drude-like, but undergoes shallow potential barriers. Using the oscillator parameters, and assuming a Fermi-velocity along the MWCNT axis, $v_F = 8 \times 10^5$ m/s,[32] we estimate the average electron scattering mean free path in the z-direction to be 3.5 ± 1.4 nm, comparable to typical scattering lengths in metals at room temperature. The Fermi-velocity in the xy-direction is not known, but should be less than 8×10^5 m/s due to the weaker coupling between electron orbitals in different shells of the MWCNT. Using this upper bound on radial velocity, we predict that the average electron scattering mean free path in the xy-direction is less than 2.4 ± 0.6 nm, much less than the typical MWCNT diameter (10–20 nm). These estimates indicate that the charge transport along the tube axis is characterized by Drude-like conduction and also supports the assumption that the transverse transport is confined within an individual CNT.

TABLE I. Uniaxial dielectric function parameters. Averaged results from 2000 independent Nelder-Mead search algorithm starting locations and their corresponding standard deviation.

ϵ_{xy}^∞	Γ_{xy} (THz)	b_{xy} (THz)	ν_{xy} (THz)
1.20 ± 0.003	339 ± 106	40 ± 6	2.2 ± 0.4
ϵ_z^∞	Γ_z (THz)	b_z (THz)	ν_z (THz)
1.2 ± 0.2	229 ± 149	51 ± 20	0.0 ± 0.01

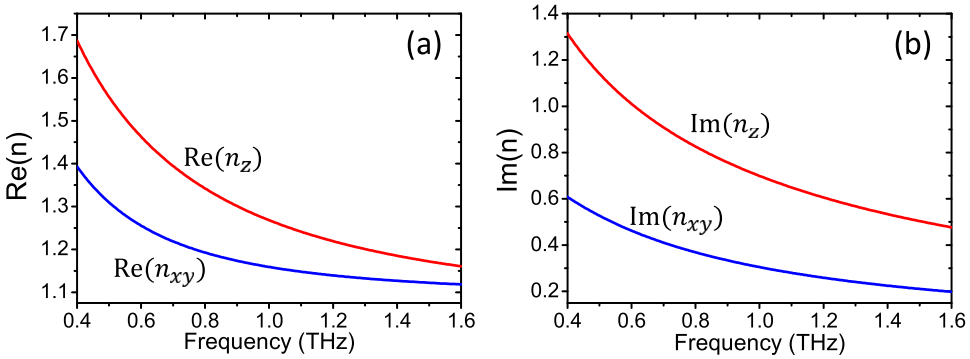

FIG. 4. (a) Real and (b) imaginary parts of the refractive index for all CNT films at THz frequencies.

Figure 4 shows the real and imaginary components of n_{xy} and n_z spectra. The anisotropic nature of the THz properties of the V-MWCNTs is evident, yet the ratio of the z-axis conductivity to the xy-axis conductivity ($\sigma_z/\sigma_{xy} \cong 2.3$, which is nearly constant over the broad spectral range, 0.4-1.6 THz) is significantly smaller than that of a SWCNT. The ratio of the V-MWCNTs is even smaller than that of graphite, $\sigma_z/\sigma_{xy} \cong 4.2$.[33] The relatively weak anisotropy of the V-MWCNT samples indicates that THz fields can readily induce electron transport between neighboring shells.

The theoretical transmission spectra, $t_{tot}(\theta, \nu)$, are used along with the incident THz electric-field spectrum in air, $a(\nu)$, to perform an inverse fourier transform to model the time-domain THz pulses

$$\tilde{E}(\theta, t) = \mathrm{Re}\left[\sum_{\omega} a(\omega) t_{tot}(\theta, \omega) e^{i(kz_0 - \omega t)}\right], \qquad (5)$$

where $t_{tot}(\theta, \omega)$ contains all the optical path length phase information for the Air-CNT-Si-Air system, and z_0 is the measurement position. Theory results shown in Figs. 3(e)–3(h) are consistent with experimental data [Figs. 3(a)–3(d)].

The experiment and theory results show that (1) the THz response along the z-axis is stronger than that of the xy-plane, yet the anisotropy is much weaker compared with that of an isolated, metallic SWCNT, (2) strong absorption in the horizontal direction indicates that charge carriers transport between adjacent shells, and (3) the z-axis THz response of MWCNTs is not overwhelmingly metallic in contrast to that of SWCNTs.[13–15] Intershell charge transports instigate scattering sites within the multi-shell structure, reducing the effective scattering length dramatically along the z-direction and introducing a significant decrease in absorption.

In conclusion, time-resolved THz transmission ellipsometry reveals the anisotropic carrier dynamics in vertically aligned MWCNTs. The conductivity along the z-axis is larger than the xy-plane, but they are the same order of magnitude. The considerably strong THz response along the xy-plane indicates that charge carrier transport occurs between neighboring shells in MWCNTs, also creating a non-negligible reduction in absorption along the length of the nanotubes. The THz ellipsometry method will also be useful to understand carrier dynamics in other nanomaterials consisting of novel two-dimensional conductors such as multilayer graphene, where transport aniosotropy is expected, yet is hard to measure with conventional electrode techniques.

This work is supported by the National Science Foundation (DMR-1063632 and ECCS-1102183) and the Oregon Nanoscience and Microtechnologies Institute. N.L.R. and K.B.K.T. acknowledge the support of the EC project TECHNOTUBES.

[1]A. Star, Y. Lu, K. Bradley, and G. Grüner, Nano Lett. **4**, 1587 (2004).
[2]J. Chen, V. Perebeinos, M. Freitag, J. Tsang, Q. Fu, J. Liu, and P. Avouris, Science **310**, 1171 (2005).
[3]M. E. Itkis, F. Borondics, A. Yu, and R. C. Haddon, Science **312**, 413 (2006).
[4]T. Fuse, Y. Kawano, T. Yamaguchi, Y. Aoyagi, and K. Ishibashi, Nanotechnology **18**, 044001 (2007).
[5]S. Watanabe, N. Minami, and R. Shimano, Opt. Express **19**, 1528 (2011).
[6]Z. Zhong, N. M. Gabor, J. E. Sharping, A. L. Gaeta, and P. L. McEuen, Nat. Nanotechnol. **3**, 201 (2008).
[7]D. Kienle and F. Léonard, Phys. Rev. Lett. **103**, 026601 (2009).
[8]T.-I. Jeon, J. Zhang, and D. Grischkowsky, Appl. Phys. Lett. **86**, 161904 (2005).
[9]I. Maeng, C. Kang, S. J. Oh, J.-H. Son, K. H. An, and Y. H. Lee, Appl. Phys. Lett. **90**, 051914 (2007).
[10]M. A. Seo, J. H. Yim, Y. H. Ahn, F. Rotermund, D. S. Kim, S. Lee, and H. Lim, Appl. Phys. Lett. **93**, 231905 (2008).
[11]T.-I. Jeon, K.-J. Kim, C. Kang, S.-J. Oh, J.-H. Son, K. H. An, D. J. Bae, and Y. H. Lee, Appl. Phys. Lett. **80**, 3403 (2002).
[12]T.-I. Jeon, K.-J. Kim, C. Kang, I. H. Maeng, J.-H. Son, K. H. An, J. Y. Lee, and Y. H. Lee, J. Appl. Phys. **95**, 5736 (2004).
[13]L. Ren, C. L. Pint, L. G. Booshehri, W. D. Rice, X. Wang, D. J. Hilton, K. Takeya, I. Kawayama, M. Tonouchi, R. H. Hauge, and J. Kono, Nano Lett. **9**, 2610 (2009).
[14]J. Kyoung, E. Y. Jang, M. D. Lima, H.-R. Park, R. O. Robles, X. Lepró, Y. H. Kim, R. H. Baughman, and D.-S. Kim, Nano Lett. **11**, 4227 (2011).
[15]L. Ren, C. L. Pint, T. Arikawa, K. Takeya, I. Kawayama, M. Tonouchi, R. H. Hauge, and J. Kono, Nano Lett. **12**, 787 (2012).
[16]Z.-P. Yang, L. Ci, J. A. Bur, S.-Y. Lin, and P. M. Ajayan, Nano Lett. **8**, 446 (2008).
[17]K. Mizuno, J. Ishii, H. Kishida, Y. Hayamizu, S. Yasuda, D. N. Futaba, M. Yumura, and K. Hata, Proc. Natl. Acad. Sci. U.S.A. **106**, 6044 (2009).
[18]S. Sanvito, Y.-K. Kwon, D. Tománek, and C. J. Lambert, Phys. Rev. Lett. **84**, 1974 (2000).
[19]S. Roche, F. Triozon, A. Rubio, and D. Mayou, Phys. Rev. B **64**, 121401 (2001).
[20]Y.-G. Yoon, P. Delaney, and S. G. Louie, Phys. Rev. B **66**, 073407 (2002).
[21]A. Hansson and S. Stafström, Phys. Rev. B **67**, 075406 (2003).
[22]K.-H. Ahn, Y.-H. Kim, J. Wiersig, and K. J. Chang, Phys. Rev. Lett. **90**, 026601 (2003).
[23]V. Zólyomi, J. Koltai, A. Rusznyák, J. Kürti, A. Gali, F. Simon, H. Kuzmany, A. Szabados, and P. R. Surján, Phys. Rev. B **77**, 245403 (2008).
[24]B. Bourlon, C. Miko, L. Forró, D. C. Glattli, and A. Bachtold, Phys. Rev. Lett. **93**, 176806 (2004).
[25]T. Wang, K. Jeppson, N. Olofsson, E. E. B. Campbell, and J. Liu, Nanotechnology **20**, 485203 (2009).
[26]Y. Saito, T. Yoshikawa, S. Bandow, M. Tomita, and T. Hayashi, Phys. Rev. B **48**, 1907 (1993).

[27]J. L. Tomaino, A. D. Jameson, J. W. Kevek, M. J. Paul, A. M. van der Zande, R. A. Barton, P. L. McEuen, E. D. Minot, and Y.-S. Lee, Opt. Express **19**, 141 (2011).
[28]A. D. Jameson, J. W. Kevek, J. L. Tomaino, M. Hemphill-Johnston, M. J. Paul, M. Koretsky, E. D. Minot, and Y.-S. Lee, Appl. Phys. Lett. **98**, 221111 (2011).
[29]P. Yeh, A. Yariv, and C.-S. Hong, J. Opt. Soc. Am. **67**, 423 (1977).
[30]D. M. Olsson and L. S. Nelson, Technometrics **17**, 45 (1975).
[31]C. T. Kelley, *Method for Optimization*, 1st ed. (Society for Industrial Mathematics, Philadelphia, 1987).
[32]A. Javey and J. Kong, in *Carbon Nanotube Electronics* (Springer, New York, 2009), Chap. 1.
[33]R. L. Powell and G. E. Childs, in *American Institute of Physics Handbook*, 3rd ed. (McGraw-Hill, New York, 1972), Chap. 4, pp. 142–160.